Applied Radiation and Isotopes 203 (2024) 111086

Contents lists available at ScienceDirect

Applied Radiation and Isotopes

journal homepage: www.elsevier.com/locate/apradiso

A novel vanadium pentoxide doped glasses characterization for radiation shielding applications

Yusuf Kavun [a,e,*], Hasan Eskalen [b,e], Mustafa Kavgacı [c,e], Hakan Yaykaşlı [d,f], Medeni Bahşi [e]

[a] Vocational School of Health Services, Department of Medical Imaging Techniques, Kahramanmaraş Sütçü İmam University, Kahramanmaras, Turkey
[b] Vocational School of Health Services, Department of Opticianry, Kahramanmaraş Sütçü İmam University, Kahramanmaraş, Turkey
[c] Elbistan Vocational School of Health Services, Department of Opticianry, Kahramanmaraş İstiklal University, Kahramanmaraş, 46300, Turkey
[d] Elbistan Vocational School of Higher Education, Kahramanmaras İstiklal University, Kahramanmaraş, Turkey
[e] Institute of Science, Department of Material Science and Engineering, Kahramanmaraş Sütçü İmam University, Kahramanmaraş, 46050, Turkey
[f] Institute of Graduate Studies, Department of Material Science and Engineering, Kahramanmaraş İstiklal University, Kahramanmaraş, Turkey

ARTICLE INFO

Keywords:
Vanadium pentoxide
Glass
Radiation shielding
TGA
XRD

ABSTRACT

Glasses are actively used in various fields, from industry to health. Especially, special doped glasses used in radiation areas may vary depending on the type and energy of the radiation. Glasses made of high-density and effective radiation-absorbing materials generally provide adequate protection against X and gamma rays. As an example, in this study, a $42.5P_2O_5$–$42.5B_2O_3$–$(15-x)Li_2O$–xV_2O_5 (x = 0, 2.5, 5, 10 and 15) glass system was produced using the melt quenching technique. The obtained X-ray patterns indicated that lack of crystalline peaks, verifying the glassy nature of all synthesized glass series. The glass transition temperatures and the glass thermal stability were determined using a Differential Thermal Analysis (TGA). The glass transition temperature and thermal stability was found to deteriorate with increasing V_2O_5 content. The radiation absorption properties of these glass system produced were investigated with 384 keV, 1173 keV and 1333 keV energized gamma using narrow beam transmission geometry. The NaI(Tl) detector system have been used to obtain γ-ray spectra. According to the obtained mass attenuation coefficients (μ_m) results, it has been determined that as the V_2O_5 ratio in the glass increases, it provides more effective results in radiation shielding. When the experimental results are compared with the theoretical XCOM results, there are a good match between the values. Finally, the radiation shielding properties of this produced glass system are compared with previously studied standard glasses to refer to the superiority of the installed systems.

1. Introduction

Understanding the impact of radiation on human health is an evolving field. Effective shielding is crucial to minimize radiation exposure from natural and artificial sources. The key principle in radiation shielding involves using a material that interacts significantly with radiation particles, causing them to lose energy through various interactions and ultimately be absorbed by the material (Knoll and Kraner, 1981) (Niksarlıoğlu et al., 2023) (Hannachi et al., 2023) (James E. Martin and Tanır G, 2013). Glass, a rare and versatile substance, possesses qualities such as rigidity, brittleness, and high compression resistance. It also exhibits resistance to chemical effects from air, water, and various acids. Composed of inorganic substances fused at high temperatures, glass primarily consists of alkalis, earthy bases, or metallic oxides of silica. It is abundant in nature in forms such as silica, flint, quartz, and sand to create glass, sand, alkali, and lead oxide must be heated to high temperatures The mixture, when heated, undergoes solvent action from fused alkali and lead oxide until it transforms into a molten glass mass (Hlavae, 1983) (Holand and Beall, 2019) (Jeager, 1975).

Vanadium, possessing five outer valence electrons, shares chemical similarities with nitrogen, phosphorus, arsenic, and antimony (Fritsch et al., 1987). Much like nitrogen, it gives rise to oxides in states of five, four, three, and potentially monovalent. Additionally, it exhibits a propensity for the formation of various vanadates—ortho-, pyro-, meta- and poly-, nearly as abundantly as the radicals formed by pentavalent phosphorus. Notably, vanadium mirrors phosphorus in its tendency to produce glassy vanadium pentoxide (Gaddam et al., 2021). In terms of

* Corresponding author. Vocational School of Health Services, Department of Medical Imaging Techniques, Kahramanmaraş Sütçü İmam University, Kahramanmaras, Turkey.
E-mail addresses: yusufkavun@gmail.com, yusufkavun@ksu.edu.tr (Y. Kavun).

https://doi.org/10.1016/j.apradiso.2023.111086
Received 2 May 2023; Received in revised form 23 October 2023; Accepted 24 October 2023
Available online 27 October 2023
0969-8043/© 2023 Elsevier Ltd. All rights reserved.

Table 1
Chemical composition of the glasses.

Glass code	Composition (mol%)				Density (g/cm^3)
	V_2O_5	Li_2O	B_2O_3	P_2O_5	
Y0	0	15	42.5	42.5	2.472
Y1	2.5	12.5	42.5	42.5	2.473
Y2	5	10	42.5	42.5	2.482
Y3	10	5	42.5	42.5	2.497
Y4	15	0	42.5	42.5	2.521

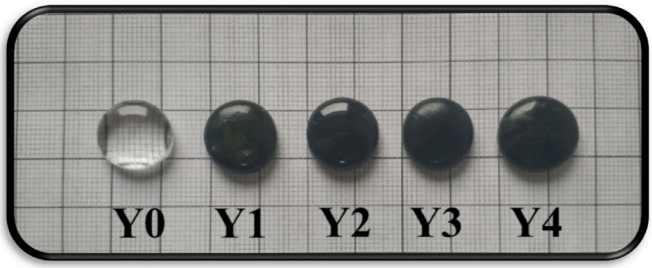

Fig. 1. Image of produced glass samples.

appearance, compounds of vanadium bear a closer resemblance to neighboring transition elements like Oria, iron, and notably, chromium. Bivalent vanadium stands out as a potent reducing agent, giving rise to salts with a distinctive lavender hue. In its oxide form, vanadium dioxide acts as an insulator, effectively retaining indoor heat while allowing the full spectrum of sunlight to permeate from the outside (Fritsch et al., 1987; Shen et al., 2021). However, at elevated surface temperatures, it undergoes a transformation into a metallic state, impeding the penetration of heat-causing infrared solar radiation (Weyl et al., 1939; Masayuki Yamane, 2004).

Boro-phosphate glasses find applications in nonlinear optics and solid-state batteries. Among these, lithium borophosphate stands out as a traditional yet highly acclaimed glass, particularly in the realm of storage batteries, owing to its distinct advantages. These batteries serve as essential energy storage solutions for both optical and electrical equipment (Alrowaili et al., 2022). Moreover, lithium-borate glasses are recognized for their capacity to maintain low production temperatures, enhanced solubility, and improved thermal stability, thanks to the robust ionic interactions among cations within the glass network. The introduction of Li_2O into these glasses leads to a transformation of bridging oxygen into non-bridging oxygen. Consequently, lithium-boro-phosphate glasses exhibit exceptional physical and chemical stability, coupled with reliable voltage performance, making them a valuable choice as solid electrolytes, especially due to their improved ionic conductivities (Madhu et al., 2023a).

The fundamental principle of radiation shielding hinges on the material's capacity to engage extensively with radiation particles. Through a series of interactions, these particles dissipate their energy, ultimately leading to their absorption by the shielding material (Krane, 1991). The Li_2O–B_2O_3–P_2O_5 glass series was synthesized and the influence of TeO_2 on its radiation shielding properties was examined. The results demonstrate that the incorporation of TeO_2 into the glass samples had a beneficial impact on their nuclear protection capabilities was reported (Susoy, 2020). Numerous studies have demonstrated the pivotal role of transition metal oxides (TMOs) in the fabrication of glass. Among these, vanadium oxide (V_2O_5) stands out as an intriguing TMO, serving as a conditioning agent to enhance the electrical, optical, and magnetic properties of the resultant glasses (Rammah et al., 2020a). To improve performance V_2O_5 -Li_2O– P_2O_5 glass system, the effects of incremental doping with a transition metal oxide (V_2O_5) on both the anticipated nonlinear and linear optical parameters was examined (Ravisankar et al., 2019). Recently, it has been reported that boron-rich glasses provide poorer radiation shielding than phosphate-rich glasses (Gomaa et al., 2021). Another study reported that as the WO_3 content in lithium borate glasses increases, there is an observed increase in the mass attenuation coefficient, effective atomic number, and stiffness values (Uosif et al., 2020). Also, vanadyl lead phosphate glasses have the potential to serve as an effective radiation shielding material was revealed from the recent study (Rammah et al., 2020b).

In this investigation, a glass system comprising $42.5P_2O_5$, $42.5B_2O_3$, and $(15-x)Li_2O$–xV_2O_5 (with x values of 0, 2.5, 5, 10, and 15) was fabricated through the melt extinguishing system technique. The produced glass system underwent irradiation using a ^{133}Ba and ^{60}Co point source with 1 mCi activity. Gamma spectra with energies of 384 keV, 1173 keV, and 1333 keV were subsequently measured utilizing a NaI(Tl) detector (Kavun et al., 2022). Comparison of the experimental outcomes with those obtained from the XCOM simulation code (Berger and Hubbell, 1987), reveals a strong alignment between the values. Finally, the radiation shielding properties of the newly developed glass system are juxtaposed with those of previously investigated standard glasses, illustrating the superiority of the implemented systems.

2. Material and method

2.1. Glasses preparation

The well-established melt-quench process was employed to fabricate V_2O_5 -doped glasses with varying compositions: x V_2O_5 - (15-x) Li_2O – 42.5 B_2O_3 – 42.5 P_2O_5, where x took values of 0, 2.5, 5, 10, and 15 mol % denoted as Y0, Y1, Y2, Y3, and Y4, respectively. The components, along with their respective quantities as listed in Table 1, were meticulously blended. This amalgam was then transferred into alumina crucibles, which were subsequently placed in the furnace, set at 1150 °C. Throughout the melting process, continuous agitation was maintained to prevent the formation of bubbles. The resulting melts were poured into steel molds and transferred to a 400 °C furnace for annealing, a process that lasted for 4 h before allowing natural cooling. In Fig. 1, visual representations of the manufactured glass samples are presented.

2.2. Characterization

Structural characterization of the synthesized glass samples was carried out by XRD device. The amorphous structure of the glasses was obtained by the X-ray diffractometer (Philips X'Pert PRO, Netherland) using Cu-kα radiation source (λ = 1.54 Å). The microhardness of the glass samples was investigated with a Shimadzu microhardness tester. The Vickers microhardness of the glasses samples was measured using a Vickers tester (Shimadzu HMV-2 Machine, Japan) for 15 s under a load of 2.942N, and the average hardness was obtained from 10 indents. The thermal properties were established by differential thermal analysis (DTA-Perkin-Elmer Sapphire, USA) in a nitrogen atmosphere. A heating rate of 15 °C/min was implemented in the temperature range of 200°C–900 °C. The chemical functionalities of the synthesized glasses were investigated by FTIR analysis. The Perkin Elmer Spectrum 400 device (USA) was used to obtain FT-IR spectra in the 4000 cm^{-1} - 400 cm^{-1} range.

2.3. γ-ray spectra

Radiation measurements were carried out in the experimental setup given in Fig. 2. Accordingly, the Linear Attenuation Coefficient (μ) (LAC) is calculated with Lambert-Beer's law (Kavun et al., 2021) given in Eq. (1). where I_0 is the gamma measured without glass in the experimental setup, and I is the gamma number measured after the glasses are placed in the experimental setup. Although x is expressed as the thickness of the glass here, the glass thicknesses are produced the same. instead, the amount of V_2O_5 in the glass changes.

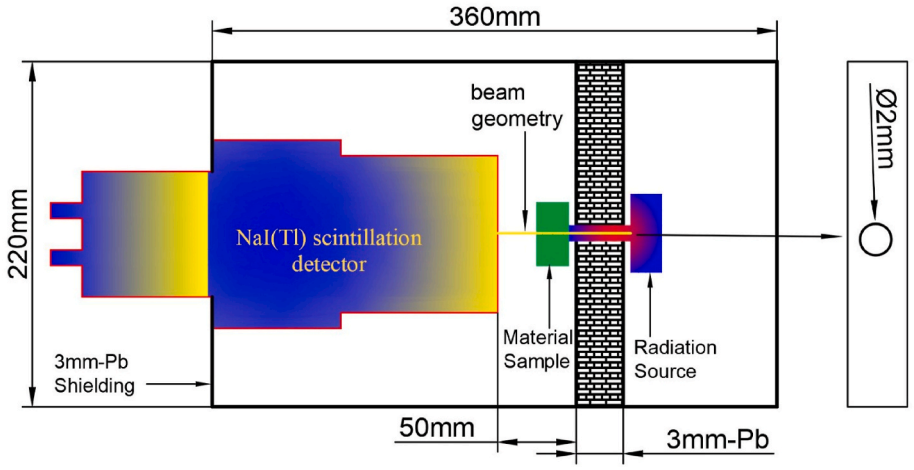

Fig. 2. Experimental schema of radiation shielding measurements.

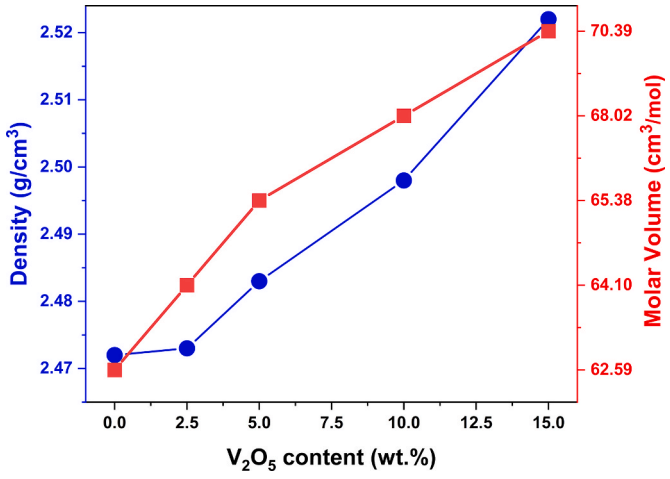

Fig. 3. Density and molar volume for the glass samples.

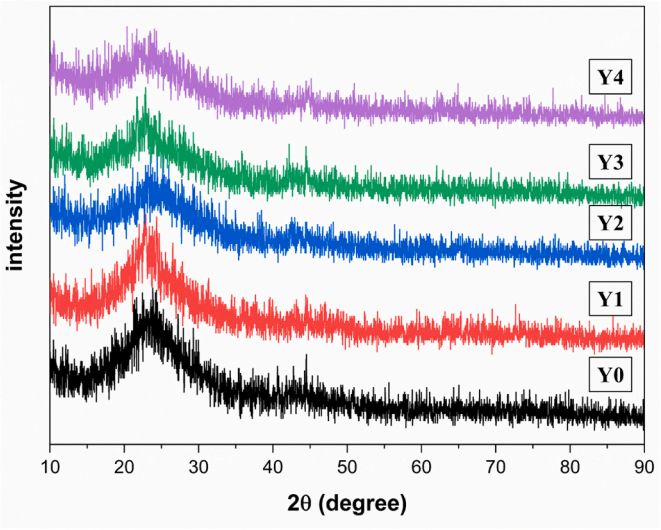

Fig. 5. X-Ray diffraction pattern of Y-series glasses.

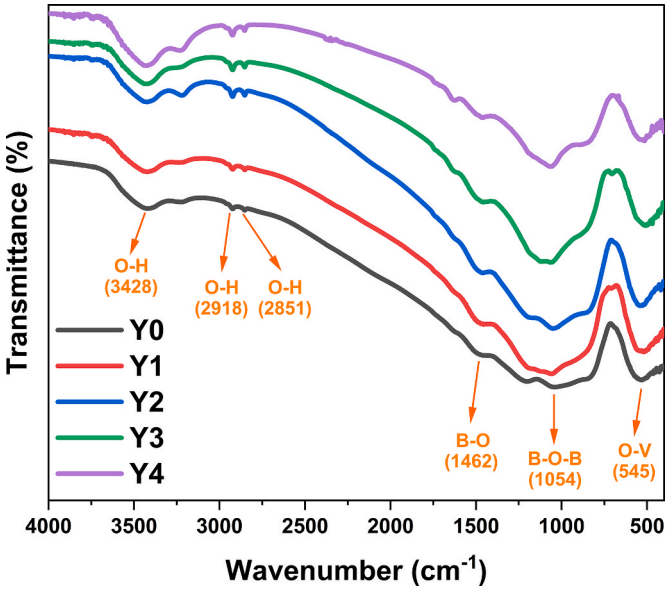

Fig. 4. FTIR spectra of glass samples.

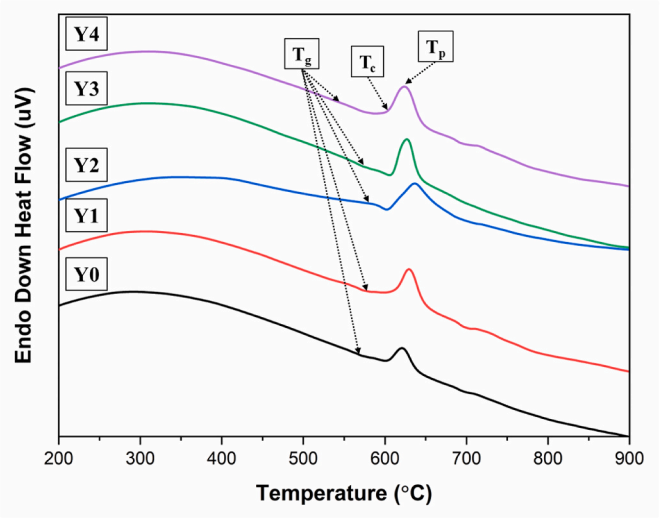

Fig. 6. DTA graphs of Y series glasses.

Table 2
DTA of the prepared glasses.

Sample Code	T_g(°C)	T_c(°C)	T_p(°C)	ΔT(°C)
Y0	572	604	622	32
Y1	575	608	628	33
Y2	583	614	636	31
Y3	581	611	625	30
Y4	549	578	624	29

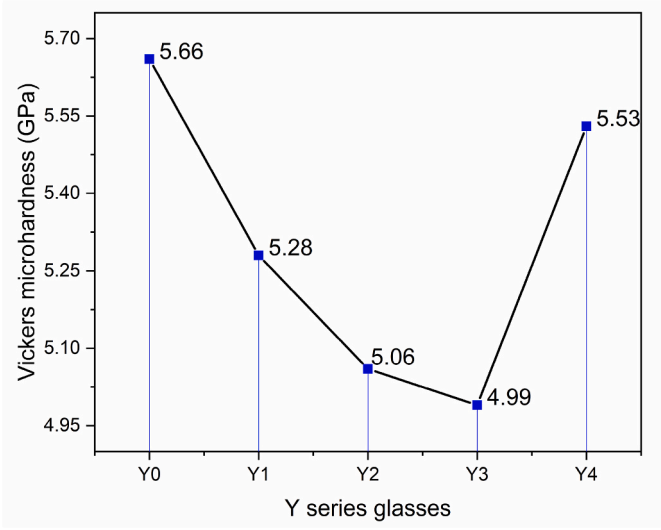

Fig. 7. Variation of micro-hardness for the $42.5P_2O_5$–$42.5B_2O_3$–(15−x) Li_2O–xV_2O_5 glasses.

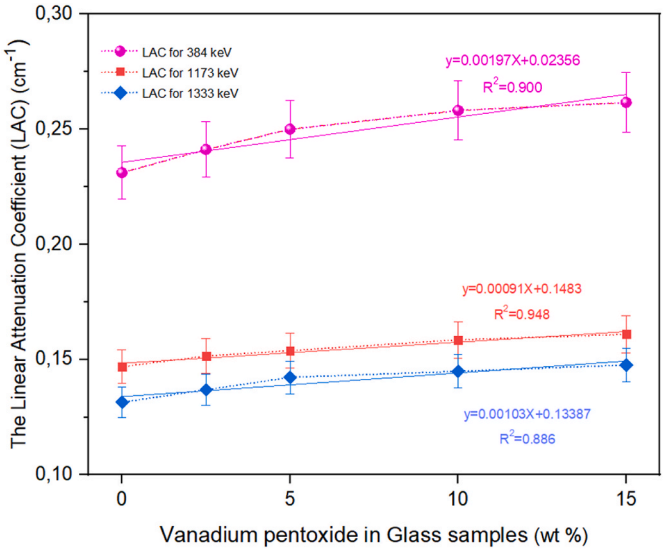

Fig. 8. μ Values of V_2O_5 doped glasses.

$$\mu = \ln\left(\frac{I_0}{I}\right) \Big/ (-x)\,(\mathrm{cm}^{-1}) \tag{1}$$

By using obtained μ, the standart deviation (Yaykaşlı et al., 2022) of these experiments have been calculated via Eq. (2):

$$\sigma = \sqrt{\frac{\sum_{i=1}^{N}(\mu_i - \overline{\mu})^2}{N-1}} \tag{2}$$

Each measurement is represented by μ_i and the average of the

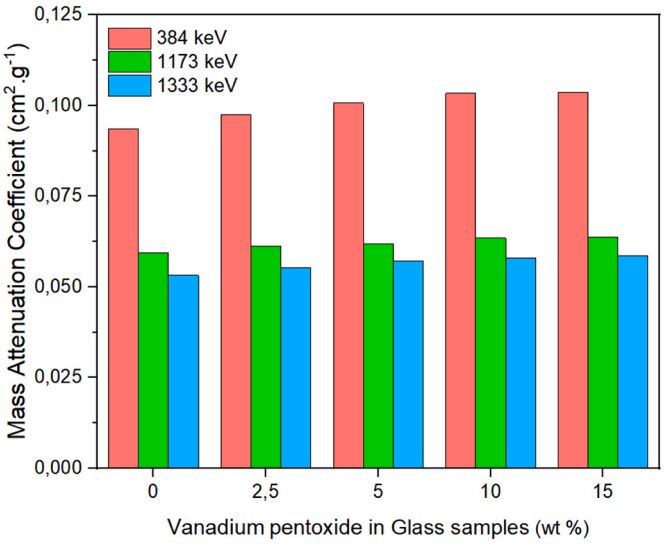

Fig. 9. The Mass attenuation coefficient values of V_2O_5 doped glasses.

measurements are represented by $\overline{\mu}$. N is the number of measurements of every glass sample. The amount of radiation absorbed by a unit mass is found by the mass attenuation coefficient and this is given in Eq. (3) (Kavun et al., 2021):

$$\mu_m = \frac{\mu}{\rho}\ (\mathrm{cm}^2/\mathrm{g}) \tag{3}$$

here, the linear attenuation coefficient is μ and density is ρ.

The material thickness that halves the incoming gamma number is calculated with Half Value Layer (HVL), and the material thickness that reduces it to one-tenth is calculated with Tenth Value Layer (TVL). These are given in Eqs. (4) and (5), respectively (Eskalen et al., 2020). The path taken by the gamma in the material is calculated with the Mean Free Path (MFP) given in Eq. (6) (Eskalen et al., 2020).

$$\textit{Half Value Layer}\ (HVL) = \frac{\ln 2}{\mu}\ (\mathrm{cm}) \tag{4}$$

$$\textit{Tenth Value Layer}\ (TVL) = \frac{\ln 10}{\mu}(\mathrm{cm}) \tag{5}$$

$$\textit{Mean Free Path}\ (MFP) = \frac{1}{\mu}(\mathrm{cm}) \tag{6}$$

^{133}Ba and ^{60}Co point source with 1 mCi activity have been used for irradiation and 384 keV, 1173 keV, and 1333 keV energized gamma have been measured by using NaI(Tl) detector system (ORTEC® 905-4) (Yaykaşlı et al., 2022). This experimental setup has been given in Fig. 2.

2.4. Density and molar volume

A 4-digit precise microbalance (Axiss ACN 220) was used to calculate the density of the glass samples using Archimedes' principle. The density of the obtained glass was calculated by using the equation;

$$\rho = \frac{w_A}{w_A - w_B}\, x\rho_{liquid}\ (\mathrm{g}/\mathrm{cm}^3) \tag{7}$$

here, ρ, w_A, w_B and ρ_{liquid} is density of glass sample, weight of obtained glass in air, weight of obtained glass in liquid and density of liquid respectively. The molar volume (V_M) of glass samples is an essential physical parameter that may be estimated using the sample's molecular weight (M) and observed density value (Mandal et al., 2023). The molar volume (V_g) of the synthesized glass might be obtained from the following equation;

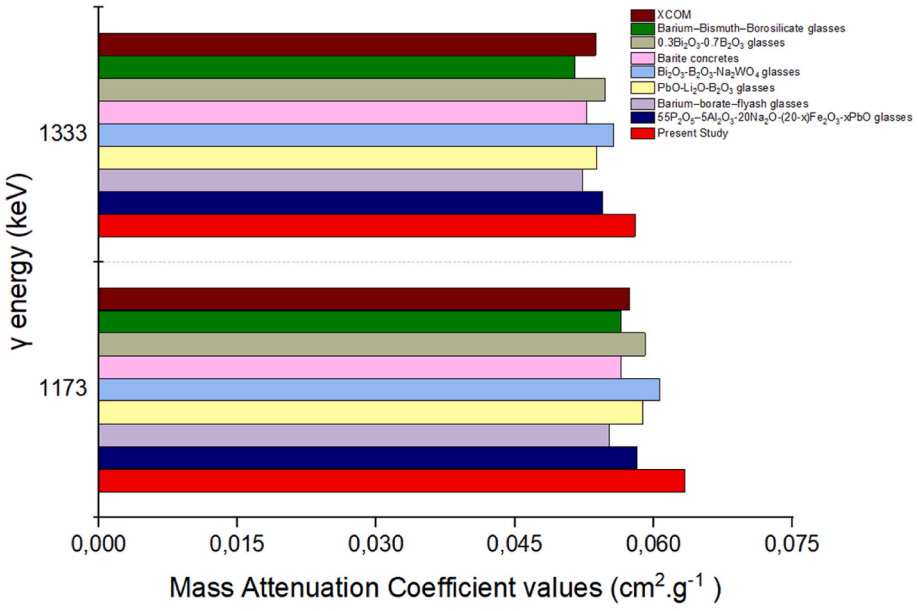

Fig. 10. The Mass attenuation coefficient comparison of some shielding materials with present 10% V_2O_5 doped glasses.

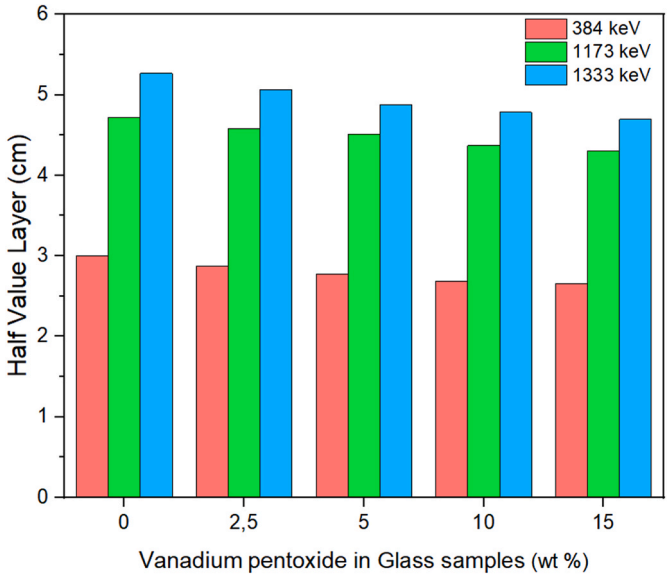

Fig. 11. Half Value Layer (HVL) values of V_2O_5 doped glasses.

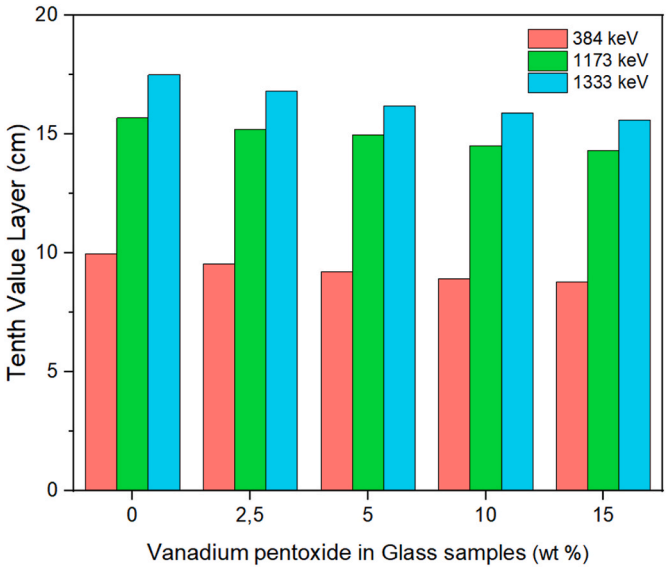

Fig. 12. Tenth Value Layer (TVL) values of V_2O_5 doped glasses.

$$V_g = \frac{M}{\rho} \ (\mathrm{cm}^3/\mathrm{mol}) \tag{8}$$

where, M is defined as molar mass.

3. Results and discussion

Fig. 3 presents the computed densities (ρ) and molar volumes (V_m) of the fabricated V_2O_5-doped glasses. With an increase in the concentration of V_2O_5 in the glass samples, the density values also showed an increment from 2.472 g/cm^3 to 2.522 g/cm^3. Comparatively, the density of Li_2O is 2.01 g/cm^3, while that of V_2O_5 is 3.36 g/cm^3. This observed rise in density in the synthesized samples as V_2O_5 content increases aligns with the theoretical expectations, confirming the experimental results. Additionally, as the mol% of V_2O_5 increased, the molar volume values of the glasses expanded from 62.59 cm^3/mol to 70.39 cm^3/mol. This suggests a proportional relationship between vanadium concentration and molar volume. This phenomenon may be attributed to the influence of polarizing power strength, which is a measure of the ratio of cation valence to its diameter (Al-Assiri, 2008).

Fig. 4 presents the 400–4000 cm^{-1} range of glass sample FTIR spectra. Visually, there was no noticeable difference between the FTIR spectra of the glass samples. Doping the glass matrix with up to 15 mol% V_2O_5 appears to have no effect on the IR peaks. It is obvious that adding up to 15 mol% V_2O_5 has no significant influence on the main characteristic groups, but it has a very tiny effect on the intensities of other IR bands (Kerkouri et al., 2011). The existence of hydroxyl groups is shown by the wide band present in all glasses about 3428 cm^{-1}, which corresponds to the essential stretching vibrations of O–H ions. The detected peaks, which are centered at 2851 cm^{-1} and 2918 cm^{-1}, are attributed to typical of hydrogen bonding in glass systems (Karunakaran et al., 2009). The peak around 1462 cm^{-1} may be caused by the B–O asymmetric stretching vibration of the BO_3 units (Kumar et al., 2019) (Singh et al., 2011). The band at 1054 cm^{-1} is due to BO_4 unit B–O–B bond stretching

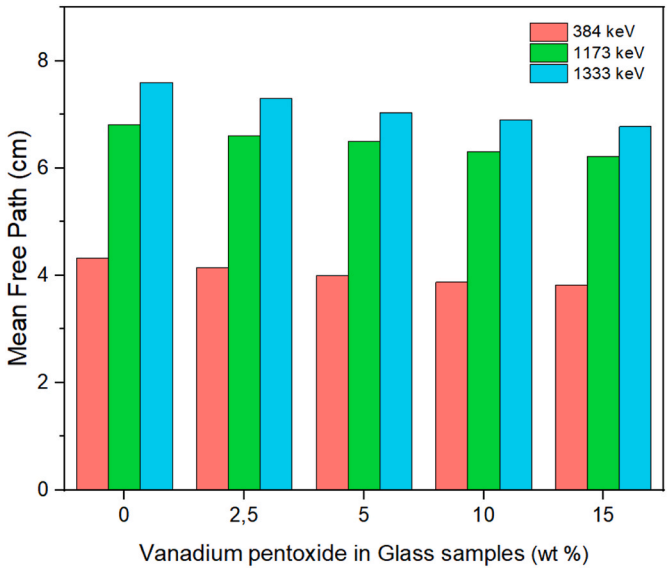

Fig. 13. Mean Free Path (MAC) values of V_2O_5 doped glasses.

vibrations (KILIÇ, 2020). Previous research has reported that the O–V angular vibration correspond to 545 cm^{-1} (KILIÇ, 2020) (Laila et al., 2013).

X-ray diffraction studies were performed between $10° \leq 2\theta \leq 90°$. Fig. 5 offers the X-ray diffraction graph of all Y-series glass systems. X-ray diffraction analysis indicated a knoll broad of about $2\theta \sim 20°–30°$, proving an amorphous structure for all Y-series glasses. The XRD graphs illustrate a fully amorphous glass structure with no sign of crystallization Y-series glasses produced. R. Divina et al. (Divina et al., 2020) reported similar XRD graph results for amorphous glass systems. In all Y series glass samples, the XRD curves are amorphous in nature of glass but different in density, indicating possible structural changes in XRD peak intensity (Nandi et al., 2022). For this reason, amorphous peaks may have partial intensity differences. The densities of the glasses produced in this study vary, and Y0 glass has the lowest density.

Fig. 6 present the DTA curves for different glasses samples. The DTA graphs for all curves indicate just one peak of exothermic. Table 2 summarizes produced of glass-transition temperature (T_g), crystallization temperature (T_c), and the peak of crystallization temperature (T_p) with the thermal parameters that can be determined by DTA analysis. Also, thermal stability has been calculated as formula $\Delta T = T_c - T_g$. The glass transition temperature of obtained glasses increases up to 10% V_2O_5. It may be explicable by the melting point of V_2O_5 (1750 °C) being higher than those of Li_2O (1438 °C), B_2O_3 (450 °C) and P_2O_5 (340 °C). All values of ΔT of Y series glasses were determined as 30 °C on average (Zhang et al., 2022). As a result, these glasses can be difficult to manufacture using traditional techniques. However, it is worth noting that the thermal stability results of these glasses are precision (El-Rehim et al., 2021) (Somaily et al., 2021). It is seen that Tg and Tc values increase by increasing the V_2O_5 concentration in Y series glasses. This may be because the inclusion of V_2O_5 into the matrix of P_2O_5 and B_2O_3 in glass samples causes structural distortion (Madhu et al., 2023b). In addition, V_2O_5 can increase T_g values by causing changes in the BO_3 and BO_4 groups (Dahiya et al., 2016). In addition, it is thought that the main reason for the difference in DTA results of Y series glasses is the binding of vanadium metal ions to the glass network and the strengthening of the system, which may cause the thermal resistance of the glasses to increase.

The Vickers microhardness of obtained $42.5P_2O_5–42.5B_2O_3–(15-x)Li_2O–xV_2O_5$ glasses are presented in Fig. 7. The hardness decreased as the V_2O_5content increased from 0% to 10%. It is seen that Y0 (5.66 GPa) and Y4 (4.99 GPa) glasses have the highest and lowest hardness values. However, no striking change was observed in the hardness values of Y series glasses with the addition of V_2O_3. As a result, it has been determined that the Y series glasses are reproducibility, and their hardness values are stable. Taha et al. It has been stated that as the CuO content increases in $P_2O_5–Li_2O–CuO$ glasses, the significant increase in hardness values is closely related to the density values of the glasses (Taha et al., 2021). It did not observe a change in the hardness results of the Y series glasses because the density values of the glasses are stable.

μ of V_2O_5 doped glasses are shown in Fig. 8. Accordingly, the μ value obtained with 384 keV energy gammas started around 0.2311±0.0116 cm^{-1} and gradually increased. This value has reached 0.2615±0.0131 cm^{-1} in 15% V_2O_5 doped glass. The R^2 value of these values was obtained as 0.900. These values decreased at 1173 keV gamma energy, but the values continued to increase according to the amount of V_2O_5. The R^2 value of these values was found to be 0.948. Finally, the μ values obtained with 1333 keV energy gammas were seen to be close to the previous μ values. The increasing trend in these μ values increased similarly to the increase in the amount of V_2O_5 at 1173 keV. The R^2 value here is determined as 0.886.

The Mass Attenuation Coefficient (MAC) results of V_2O_5 doped glasses are shown in Fig. 9. As can be seen from the MAC results in Fig. 9, the MAC values at 384 keV gamma energy were obtained as the highest at all V_2O_5 concentration values. The values, which were around 0.0934 $cm^2\ g^{-1}$ at this energy, decreased slightly at 1173 keV gamma energy and decreased to around 0.0593 $cm^2\ g^{-1}$. Finally, it was measured at around 0.0532 $cm^2\ g^{-1}$ at an energy of 1333 keV. Accordingly, as the gamma

Table 3
The shielding parameters of V_2O_5 doped Glass samples.

Concentration	μ (384 keV)	ρ	HVL	TVL	MFP	MAC $_{Exp.}$	MAC $_{XCOM}$	$\Delta_{XCOM-Exp.}$
0% V_2O_5	0.2311±0.0116	2.4720	2.9992	9.9631	4.3269	0.0934±0.0031	0.0944	0.98%
2.5% V_2O_5	0.2411±0.0121	2.4732	2.8742	9.5479	4.1466	0.0975±0.0011	0.0945	3.23%
5% V_2O_5	0.2499±0.0125	2.4828	2.7731	9.2120	4.0007	0.1006±0.0005	0.0945	6.52%
10% V_2O_5	0.2581±0.0129	2.4975	2.6852	8.9199	3.8739	0.1033±0.0018	0.0946	9.27%
15% V_2O_5	0.2615±0.0131	2.5215	2.6499	8.8029	3.8231	0.1037±0.0020	0.0947	9.56%
	μ (1173 keV)							
0% V_2O_5	0.1468±0.0073	2.4720	4.7212	15.6836	6.8113	0.0593±0.0013	0.0573	3.61%
2.5% V_2O_5	0.1514±0.0076	2.4732	4.5759	15.2009	6.6017	0.0612±0.0004	0.0573	6.83%
5% V_2O_5	0.1538±0.0077	2.4828	4.5063	14.9697	6.5013	0.0619±0.000008	0.0574	8.03%
10% V_2O_5	0.1585±0.0079	2.4975	4.3729	14.5264	6.3087	0.0634±0.0007	0.0574	10.61%
15% V_2O_5	0.1608±0.0080	2.5215	4.3088	14.3136	6.2163	0.0637±0.0009	0.0574	11.14%
	μ (1333 keV)							
0% V_2O_5	0.1315±0.0066	2.4720	5.2695	17.5048	7.6022	0.0532±0.0016	0.0537	0.91%
2.5% V_2O_5	0.1368±0.0068	2.4732	5.0647	16.8245	7.3068	0.0553±0.0006	0.0537	3.03%
5% V_2O_5	0.1422±0.0071	2.4828	4.8742	16.1918	7.0320	0.0572±0.0004	0.0537	6.60%
10% V_2O_5	0.1448±0.0072	2.4975	4.7839	15.8918	6.9017	0.0580±0.0008	0.0538	7.91%
15% V_2O_5	0.1475±0.0074	2.5215	4.6967	15.6020	6.7758	0.0585±0.0010	0.0538	8.81%

energy value increased, the MAC value decreased. As can be seen from here, the energy value and MAC value are inversely proportional.

The Mass Attenuation Coefficient (MAC) values comparison measured at 1173 keV and 1333 keV energies can be seen in Fig. 10. Accordingly, the obtained MAC values of 10%V_2O_5 doped glasses were higher than the other materials at 1173 keV and 1333 keV energies. For example, for 55P_2O_5–5Al_2O_3-20 Na_2O-(20-x)Fe_2O_3-xPbO glasses, the MAC value have been obtained as 0.0582 cm^2 g^{-1} at 1173 keV gamma energy and also it was found as 0.0545 cm^2 g^{-1} at 1333 keV (El-Taher et al., 2019). The MAC values have been found as 0.0565 cm^2 g^{-1} and 0.0528 cm^2 g^{-1} for barite concretes (Dogra et al., 2017) at same energies. For Barium–borate–fly ash glasses (Singh et al., 2008), the MAC values were obtained as 0.0552 cm^2 g^{-1} and 0.0523 cm^2 g^{-1}. To PbO–Li_2O–B_2O_3 glasses (Kumar, 2017), 0.0589 cm^2 g^{-1} and 0.0539 cm^2 g^{-1} MAC values have been obtained for 1173 keV and 1333 keV. The MAC values were found for Bi_2O_3–B_2O_3–Na_2WO_4 glasses (Dogra et al., 2017) as 0.0589 cm^2 g^{-1} and 0.0539 cm^2 g^{-1} MAC for same energies. The Barium–Bismuth–Borosilicate glasses (Bootjomchai et al., 2012) have 0.0565 cm^2 g^{-1} and 0.0515 g cm^{-2} MAC values for 1173 keV and 1333 keV energies, respectively. The MAC values of 10% V_2O_5 doped glasses were calculated theoretically by XCOM (Berger and Hubbell, 1987) by means of gammas with 1173 and 1333 keV energies. Accordingly, the MAC value found to be 0.05738 cm^2 g^{-1} at 1173 keV energy was calculated as 0.05376 cm^2 g^{-1} at 1333 keV. Finally, 0.3Bi_2O_3-0.7B_2O_3 glasses (Dogra et al., 2017) 0.0591 cm^2 g^{-1} and 0.0548 cm^2 g^{-1} for same energies. But the present study for 10% V_2O_5 doped glasses have 0.0634 ±0.0007 cm^2. g^{-1} value at 1173 keV and 0.0580±0.0008 cm^2. g^{-1} value at 1333 keV.

In Fig. 11, the Half Value Layer (HVL) values of V_2O_5 doped glasses are shown. This value, which indicates the amount of glass thickness that can transmit half of the gamma radiation that interacts with glass, was measured to be highest at 1333 keV energy. However, as the amount of V_2O_5 in the glass increased, this value decreased slightly. At 1173 keV energy, this HVL values decreased slightly, and at 384 keV energy, the required glass thickness and amount of glass was determined to be the lowest compared to the others and can be seen in Fig. 11.

TVL values, which express the material thickness required to reduce the amount of radiation interacting with the material to one-tenth, are given in Fig. 12. As in the previous figure where HVL values are shown, in Fig. 12 where TVL values are shown, the glass thickness that will reduce the gamma amount to one-tenth was obtained as the highest at 1333 keV. As the amount of V_2O_5 in the glass increases, these values decrease again. As the energy value decreases, the required glass thickness decreases. From here, the effect of the energy value on the thickness can be clearly seen. From here, the effect of the energy value on the thickness can be clearly seen.

MFP values expressing the path that gamma can take in the material are shown in Fig. 13. Here, similar to the previous HVL and TVL figures, MFP, which is the expression of the path that gammas can take in glass, is highest at 1333 keV energy. These values decrease as the amount of energy decreases. As can be understood from here, the energy of gamma directly affects the MFP. The experimentally measured and theoretically calculated shielding parameters have been given in Table 3.

4. Conclusion

In this study, some physical properties of 42.5P_2O_5–42.5B_2O_3–(15−x)Li_2O–xV_2O_5 (x = 0, 2.5, 5, 10 and 15) glasses and V_2O_5 dope to these glasses, potential radiation shielding properties were tried to be revealed. For this purpose, some analyzes revealing XRD, FTIR, DTA, micro-hardness and radiation shielding properties were performed.

Here, Linear Attenuation Coefficient (LAC) values were determined experimentally by means of gamma with energies of 384 keV, 1173 keV and 1333 keV via NaI(Tl) detector system (ORTEC® 905-4).

By experimentally determining the μ value, the Mass Attenuation Coefficients (MAC) of these glasses were also calculated and it was determined that the MAC values in each energy group increased as the amount of V_2O_5 in the glass increased. In addition, MAC values theoretically calculated with XCOM also showed a similar increase. However, the experimental MAC values we obtained gave better results than both the theoretical XCOM and many shielding material examples in the literature at 1173 and 1333 keV energy, as seen in Fig. 10.

Another shielding parameter, HVL, TVL and MFP, similarly decreased with the increase in the amount of V_2O_5 in the glass and revealed that these glasses can be used in radiation shielding.

CRediT authorship contribution statement

Yusuf Kavun: Writing – original draft, Supervision, Methodology, Investigation, Formal analysis, Data curation, Conceptualization. **Hasan Eskalen:** Validation, Methodology, Conceptualization, Visualization, Writing – review & editing. **Mustafa Kavgacı:** Visualization, Resources, Data curation, Investigation, Writing – review & editing. **Hakan Yaykaşlı:** Visualization, Resources, Data curation, Investigation, Writing – original draft. **Medeni Bahşi:** Investigation.

Declaration of competing interest

The authors declare that they have no known competing financial interests or personal relationships that could have appeared to influence the work reported in this paper.

Data availability

Data will be made available on request.

Acknowledgment

This study was supported by the Scientific Research Projects Coordination Unit of Kahramanmaraş Sütçü İmam University. Project numbers 2020/7–18 M, 2020/7–19 M, 2020/7–21 M and 2021/3-2 YLS.

References

Al-Assiri, M.S., 2008. Characterization and electrical properties of V2O5–CuO–P2O5 glasses. Phys. B Condens. Matter 403, 2684–2689. https://doi.org/10.1016/J.PHYSB.2008.01.049.

Alrowaili, Z.A., Ali, A.M., Al-Baradi, A.M., Al-Buriahi, M.S., Wahab, E.A.A., Shaaban, K.S., 2022. A significant role of MoO3 on the optical, thermal, and radiation shielding characteristics of B2O3–P2O5–Li2O glasses. Opt. Quant. Electron. 54, 1–19. https://doi.org/10.1007/S11082-021-03447-0/FIGURES/17.

Berger, M.J., Hubbell, J.H., 1987. XCOM: Photon Cross Sections on a Personal Computer. https://doi.org/10.2172/6016002.

Bootjomchai, C., Laopaiboon, J., Yenchai, C., Laopaiboon, R., 2012. Gamma-ray shielding and structural properties of barium–bismuth–borosilicate glasses. Radiat. Phys. Chem. 81, 785–790. https://doi.org/10.1016/J.RADPHYSCHEM.2012.01.049.

Dahiya, M.S., Khasa, S., Agarwal, A., 2016. Structural, optical and thermal properties of transition metal ions doped bismuth borate glasses. Eur. J. Glasses Sci. Technol. B Phys. Chem. Glasses 57, 45–52. https://doi.org/10.13036/17533562.57.2.023.

Divina, R., Sathiyapriya, G., Marimuthu, K., Askin, A., Sayyed, M.I., 2020. Structural, elastic, optical and γ-ray shielding behavior of Dy3+ ions doped heavy metal incorporated borate glasses. J. Non-Cryst. Solids 545, 120269. https://doi.org/10.1016/J.JNONCRYSOL.2020.120269.

Dogra, M., Singh, K.J., Kaur, K., Anand, V., Kaur, P., 2017. Gamma ray shielding and structural properties of Bi2O3-B2O3-Na2WO4 glass system. Univ. J. Phys. Appl. 11, 190–195. https://doi.org/10.13189/UJPA.2017.110508.

El-Rehim, A.F.A., Ali, A.M., Zahran, H.Y., Yahia, I.S., Shaaban, K.S., 2021. Spectroscopic, structural, thermal, and mechanical properties of B2O3-CeO2-PbO2 glasses. J. Inorg. Organomet. Polym. Mater. 31, 1774–1786. https://doi.org/10.1007/s10904-020-01799-w.

El-Taher, A., Ali, A.M., Saddeek, Y.B., Elsaman, R., Algarni, H., Shaaban, K.S., Amer, T.Z., 2019. Gamma ray shielding and structural properties of iron alkali alumino-phosphate glasses modified by PbO. Radiat. Phys. Chem. 165, 108403 https://doi.org/10.1016/J.RADPHYSCHEM.2019.108403.

Eskalen, H., Kavun, Y., Kerli, S., Eken, S., 2020. An investigation of radiation shielding properties of boron doped ZnO thin films. Opt. Mater. 105, 109871 https://doi.org/10.1016/j.optmat.2020.109871.

Fritsch, E., Babonneau, F., Sanchez, C., Calas, G., 1987. Vanadium incorporation in silica glasses. J. Non-Cryst. Solids 92, 282–294. https://doi.org/10.1016/S0022-3093(87)80046-7.

Gaddam, A., Allu, A.R., Fernandes, H.R., Stan, G.E., Negrila, C.C., Jamale, A.P., Méar, F. O., Montagne, L., Ferreira, J.M.F., 2021. Role of vanadium oxide on the lithium silicate glass structure and properties. J. Am. Ceram. Soc. 104, 2495–2505. https://doi.org/10.1111/JACE.17671.

Gomaa, H.M., Zahran, H.Y., Yahia, I.S., 2021. Influence of the structural matrix on the attenuation parameters of some iron-borophosphate glasses. J. Mater. Sci. Mater. Electron. 32, 21135–21154. https://doi.org/10.1007/S10854-021-06613-Y/FIGURES/11.

Hannachi, E., Sayyed, M.I., Slimani, Y., Elsafi, M., 2023. Structural, optical and radiation shielding peculiarities of strontium titanate ceramics mixed with tungsten nanowires: an experimental study. Opt. Mater. 135, 113317 https://doi.org/10.1016/J.OPTMAT.2022.113317.

Hlavae, J., 1983. Technology of Glass and Ceramics. Elsevier Science Pub., New York, NY, Golden, CO https://doi.org/10.2172/850486.

Holand, Wolfram, Beall, G.H., 2019. Glass-Ceramic Technology. John Wiley & Sons, Incorporated.

Jeager, R.G., 1975. Engineering Compendium on Radiation Shielding Vol. 2. Shielding Materials. Springer-Verlag New York Inc.

Karunakaran, R.T., Marimuthu, K., Surendra Babu, S., Arumugam, S., 2009. Structural, optical and thermal investigations on Dy3+ doped NaF–Li2O–B2O3 glasses. Phys. B Condens. Matter 404, 3995–4000. https://doi.org/10.1016/J.PHYSB.2009.07.160.

Kavun, Y., Eskalen, H., Kerli, S., Kavgaci, M., 2021. Fabrication and characterization of GdxFe2O3(100-x)/PVA (x=0, 5, 10, 20) composite films for radiation shielding. Appl. Radiat. Isot. 177, 109918 https://doi.org/10.1016/J.APRADISO.2021.109918.

Kavun, Y., Kerli, S., Eskalen, H., Kavgaci, M., 2022. Characterization and nuclear shielding performance of Sm doped In_2O_3 thin films. Radiat. Phys. Chem. 194, 110014 https://doi.org/10.1016/j.radphyschem.2022.110014.

Kerkouri, N., Haddad, M., Et-Tabirou, M., Chahine, A., Laânab, L., 2011. FTIR, Raman, EPR and optical absorption spectral studies on V2O5-doped cadmium phosphate glasses. Phys. B Condens. Matter 406, 3142–3148. https://doi.org/10.1016/J.PHYSB.2011.04.057.

Kiliç, G., 2020. Synthesis and optical, thermal, structural investigation of zinc-borate glasses containing V2O5. Adıyaman Üniversitesi Fen Bilimleri Dergisi 10, 307–325. https://doi.org/10.37094/ADYUJSCI.678938.

Knoll, G.F., Kraner, H.W., 1981. Radiation detection and measurement. Proc. IEEE. https://doi.org/10.1109/PROC.1981.12016.

Krane, K.S., 1991. Introductory Nuclear Physics. John Wiley & Sons.

Kumar, A., 2017. Gamma ray shielding properties of PbO-Li2O-B2O3 glasses. Radiat. Phys. Chem. 136, 50–53. https://doi.org/10.1016/J.RADPHYSCHEM.2017.03.023.

Kumar, A., Ali, A.M., Sayyed, M.I., Aşkın, A., Rashad, M., Algarni, H., 2019. Structural, optical, and gamma-ray-sensing characterization of (35 −x) PbO–10 MgO–10Na2O–5 Fe2O3–10 BaO–(30 −x) B2O3 glasses. Appl. Phys. Mater. Sci. Process 125, 1–9. https://doi.org/10.1007/S00339-019-2810-7/FIGURES/10.

Laila, S., Supardan, S.N., Yahya, A.K., 2013. Effect of ZnO addition and concurrent reduction of V2O5 on network formation and elastic properties of lead vanadate (55 −x) V2O5–45PbO–(x)ZnO glass system. J. Non-Cryst. Solids 367, 14–22. https://doi.org/10.1016/J.JNONCRYSOL.2013.02.007.

Madhu, A., El-Gawaad, N.S.A., Abdallah, S.A.O., Dadami, S.T., Hegde, B.G., Uthayakumar, T., Kumar, M.B.K., N, S., 2023a. Unravelling the conductivity behaviour of thermally stable Li2O– Bi2O3–B2O3–P2O5 glasses embedded with V2O5. Ceram. Int. 49, 28781–28793. https://doi.org/10.1016/J.CERAMINT.2023.06.138.

Madhu, A., El-Gawaad, N.S.A., Abdallah, S.A.O., Dadami, S.T., Hegde, B.G., Uthayakumar, T., Kumar, M.B.K., N, S., 2023b. Unravelling the conductivity behaviour of thermally stable Li2O– Bi2O3–B2O3–P2O5 glasses embedded with V2O5. Ceram. Int. 49, 28781–28793. https://doi.org/10.1016/J.CERAMINT.2023.06.138.

Mandal, A., Modak, N., Rakshit, A., Mondal, R., Das, A.S., Kabi, S., Mondal, S., Biswas, D., 2023. Structural modifications, optical response, and electrical conductivity mechanism of Bi2O3 doped in P2O5–V2O5–MoO3 nanocomposite glass systems. Mater. Chem. Phys. 298, 127466 https://doi.org/10.1016/J.MATCHEMPHYS.2023.127466.

Martin, James E., Tanır, G., 2013. Radyasyon Ve Radyasyondan Korunma Fiziği : Sağlık Fiziği Uygulamalı, 2020th ed. Palme Yayıncılık.

Masayuki Yamane, Y.A., 2004. Glasses for Photonics. Cambridge University Press.

Nandi, P., Dutta, D., Sanyal, B., Mishra, R., Goswami, M., Arya, A.K., 2022. Structure-property correlation study of gamma irradiated BaO-PbO-K2O-B2O3-SiO2 glasses. J. Non-Cryst. Solids 595, 121833. https://doi.org/10.1016/J.JNONCRYSOL.2022.121833.

Niksarlıoğlu, S., Akman, F., Pekdemir, M.E., Yalçın Kuzu, S., Kaçal, M.R., Yılmaz, M., 2023. An extensive investigation on gamma shielding properties of PLA/Gd2O3 nanocomposites. Radiat. Phys. Chem. 208, 110936 https://doi.org/10.1016/J.RADPHYSCHEM.2023.110936.

Rammah, Y.S., El-Agawany, F.I., Mahmoud, K.A., El-Mallawany, R., Ilik, E., Kilic, G., 2020a. FTIR, UV–Vis–NIR spectroscopy, and gamma rays shielding competence of novel ZnO-doped vanadium borophosphate glasses. J. Mater. Sci. Mater. Electron. 31, 9099–9113. https://doi.org/10.1007/S10854-020-03440-5/FIGURES/15.

Rammah, Y.S., Mahmoud, K.A., Sayyed, M.I., El-Agawany, F.I., El-Mallawany, R., 2020b. Novel vanadyl lead-phosphate glasses: P2O5–PbO–ZnONa2O–V2O5: synthesis, optical, physical and gamma photon attenuation properties. J. Non-Cryst. Solids 534, 119944. https://doi.org/10.1016/J.JNONCRYSOL.2020.119944.

Ravisankar, V., Ramesh, V., Gunasekaran, B. - al, Hussien, I.I., Mohsen, M., Hosny, H.M., Abd El Keriem, M.S., 2019. Study of the optical properties of V2O5-Li2O-P2O5 glass system. J. Phys. Conf. Ser. 1253, 012018 https://doi.org/10.1088/1742-6596/1253/1/012018.

Shen, N., Chen, S., Huang, R., Huang, J., Li, J., Shi, R., Niu, S., Amini, A., Cheng, C., 2021. Vanadium dioxide for thermochromic smart windows in ambient conditions. Mater. Today Energy 21, 100827. https://doi.org/10.1016/J.MTENER.2021.100827.

Singh, S., Kumar, A., Singh, D., Thind, K.S., Mudahar, G.S., 2008. Barium–borate–flyash glasses: as radiation shielding materials. Nucl. Instrum. Methods Phys. Res. B 266, 140–146. https://doi.org/10.1016/j.nimb.2007.10.018.

Singh, G.P., Kaur, P., Kaur, S., Singh, D.P., 2011. Role of V 2 O 5 In Structural Properties Of V 2 O 5-MnO 2-PbO-B 2 O 3 Glasses.

Somaily, H.H., Shaaban, K.S., Makhlouf, S.A., Algarni, H., Hegazy, H.H., Wahab, E.A.A., Shaaban, E.R., 2021. Comparative studies on polarizability, optical basicity and optical properties of lead borosilicate modified with titania. J. Inorg. Organomet. Polym. Mater. 31, 138–150. https://doi.org/10.1007/s10904-020-01650-2.

Susoy, G., 2020. Effect of TeO2 additions on nuclear radiation shielding behavior of Li2O–B2O3–P2O5–TeO2 glass-system. Ceram. Int. 46, 3844–3854. https://doi.org/10.1016/J.CERAMINT.2019.10.108.

Taha, M.A., Youness, R.A., El-Bassyouni, G.T., Azooz, M.A., 2021. FTIR spectral characterization, mechanical and electrical properties of P2O5-Li2O-CuO glass-ceramics. Silicon 13, 3075–3084. https://doi.org/10.1007/S12633-020-00661-5/METRICS.

Uosif, M.A.M., Mostafa, A.M.A., Issa, S.A.M., Tekin, H.O., Alrowaili, Z.A., Kilicoglu, O., 2020. Structural, mechanical and radiation shielding properties of newly developed tungsten lithium borate glasses: an experimental study. J. Non-Cryst. Solids 532, 119882. https://doi.org/10.1016/J.JNONCRYSOL.2019.119882.

Weyl, W.A., Pincus, A.G., Badger, A.E., 1939. Vanadium as a glass colorant. J. Am. Ceram. Soc. 22, 374–377. https://doi.org/10.1111/J.1151-2916.1939.TB19483.X.

Yaykaşlı, H., Eskalen, H., Kavun, Y., Gögebakan, M., 2022. Microstructural, thermal, and radiation shielding properties of Al50B25Mg25 alloy prepared by mechanical alloying. J. Mater. Sci. Mater. Electron. 33, 2350–2359. https://doi.org/10.1007/s10854-021-07434-9.

Zhang, X., Zhang, J., Zhou, C., Li, L., Qi, X., 2022. Optical properties and irradiation resistance of novel high-entropy oxide glasses La2O3-TiO2-Nb2O5-WO3-M2O3 (M=B/Ga/In). J. Rare Earths 3. https://doi.org/10.1016/j.jre.2022.04.003.